Chapter 6 Quantum Storage Devices

Chapter 6 .1 Background

Self-consistent solutions to the Schrödinger and Poisson equations have been widely used to identify both qualitative, and with varying degrees of success, quantitative behavior of DBRTDs[1,2]. Self-consistent solutions are essential because quantum well diodes often incorporate lightly doped layers, and the resulting space-charge effects can significantly influence device characteristics[3,4].

In device structures that contain N$^-$ / N++ / N$^-$ doped layers in close proximity to heterobarriers as opposed to the usual lightly doped layers calculations based on both Schrödinger-Poisson and Wigner-Poisson models result in multiple self-consistent solutions, even at zero bias [19-22,59-61]. Each solution produces a distinct current-voltage (I-V) curve that extends continuously across zero bias. This new behavior is distinctly different from the N or S-type I-V characteristics typical of normal DBRTDs. Several double barrier device structures embedded between layers that incorporate the N$^-$ / N++ / N$^-$ scheme have been fabricated in the GaAs/AlAs material system where this multi-state behavior was experimentally verified[20]. These devices can be reversibly switched between two distinct conduction curves and exhibit memory switching behavior at room temperature. This device is refered to as a Quantum Storage Device (QSD). Experimental findings indicate that these states remain stable even under short circuit conditions and can only be switched from one state to another with the application of bias in excess of certain threshold voltages. Furthermore, calculations using a self-consistent coherent tunneling model

indicate that it is possible to design QSD cells with more than two states, creating the possibility of multi-state logic and multi-bit storage. Conventional quantum well diodes without the N⁻ / N++ / N⁻ layers do not show evidence of multiple conduction curve phenomena. The new multi-state behavior has been observed to occur in devices with thin heterobarrier structure in close proximity to a large space charge region.

The QSD is a promising new quantum structure that should have digital circuit application. For instance, the QSD can be used as a memory cell. However, unlike MOS devices, the QSD does not rely on the storage of charge on a capacitor to retain its memory. Instead, it can be envisioned as a multi-discrete valued resistor which can be programmed by application of an appropriate bias. The state of the device is maintained even after all bias is removed. The device is based on quantum interference effects, which should scale to extremely small areas. It is thoght that memory circuits could be fabricated in which the total number of components per cell is only one, directly addressed in a row/column configuration. This compares with two components per cell (the storage capacitor and the gate transistor) found in standard MOS dynamic memories.

QSDs are functionally dissimilar to Shockley diodes, which also change resistance at a breakover voltage but return to the original resistance at low voltage. The distinct differential resistance corresponding to each state in a QSD is retained even at zero bias until another switching voltage is applied, at which point it changes to that associated with the other state.

The potential advantages of the QSD over existing technologies are significant. First, the QSD can be scaled down to the limit of the photolithography system. From our initial findings, we believe that the cell should work at very small geometries creating the possibilities of extremely high density memory or logic. Compared to other mesoscopic devices, the QSD operates at room temperature. Furthermore, there is a possibility that the QSD can serve as a static, non-volatile memory element or logic device with zero holding power, since multiple conduction states are stable for extended periods of time even when completely disconnected from any power supply. Finally, since the QSD is a simple two dimensional structure, memory cells may be stacked on top of each other. This fact, coupled with the possibility of more than two conduction states per cell, offers other possibilities of achieving very high densities.

Chapter 6 .2 Memory Switching Phenomena in Quantum Well Diodes

A variety of self-consistent tunneling models have shown multiple conduction states exist in diodes that combine thin heterobarriers in close proximity with $N^- / N^+ / N^-$ doped layers. A prototypical asymmetric QSD using a double barrier quantum well is shown in Figure Chapter 6 .1. This device has been grown on a Varian Gen II MBE system and fabricated using standard methods. The double barrier quantum well structure consists of an 18 monolayer (ML) lightly doped n-type (10^{16} cm^{-3}) GaAs quantum well sandwiched between nominally symmetric 6 ML unintentionally doped AlAs barriers. Background doping is believed to be n-type with an ionized doner concentration of about 10^{16} cm^{-3}. On top of the quantum well is an 18 ML n-type (10^{16} cm^{-3}) GaAs layer, 43

ML N++ (4×10^{18} cm^{-3}) GaAs layer, and 65 ML n-type (10^{16} cm^{-3}) GaAs layer. The doping sequence is crucial to device operation.

We have experimentally observed multiple, stable room temperature I-V curves in this device, as shown in Figure 2.5[13].This QSD can be repetitively switched between states by the application of an appropriate threshold voltage in this case around 1.2 volts.
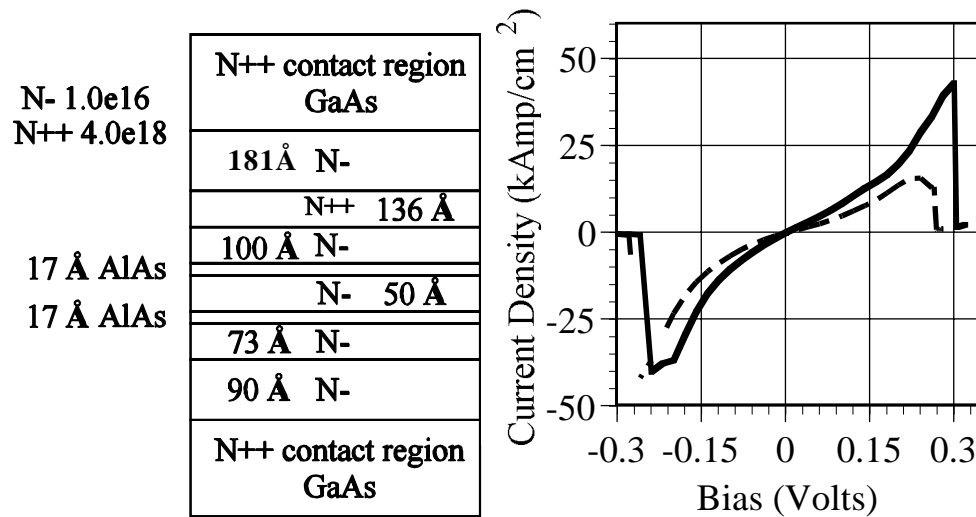

Figure Chapter 6 .1: A QSD structure is shown on the left and currents from Schrödinger Poisson self-consistent simulations of this structure are shown on the right.

Schrödinger - Poisson self-consistent simulation of the device structure in Figure Chapter 6 .1 shows multiple I/V curves that qualitatively match the experimental measurements. Note that the active regions of the device extend over only a few thermal wavelengths, and the assumption of coherent transport should be valid. Multiple solutions result only if interference effects are included in the simulation. Identical structures that omit the N++ doped layer show no

evidence of multiple solutions. The conduction band edges and electron densities at zero bias for three self-consistent solutions, together with the doping profile in the device, are shown in the left panel of Figure Chapter 6 .2. Note that the main differences between the solutions occur in the thin N++ doped layer. The self-consistent concentrations are shown for both solutions in the right panel in Figure Chapter 6 .2 and are different by about 6.9×10^{17} cm^{-3} in the N++ layer. In addition, the electron concentration tends to be more oscillatory because of the inclusion of different concentrations in resonances and quasi-bound states. Simulations based on the tight binding approximation have shown poor convergence for solutions containing quasi-bound states for this structure.
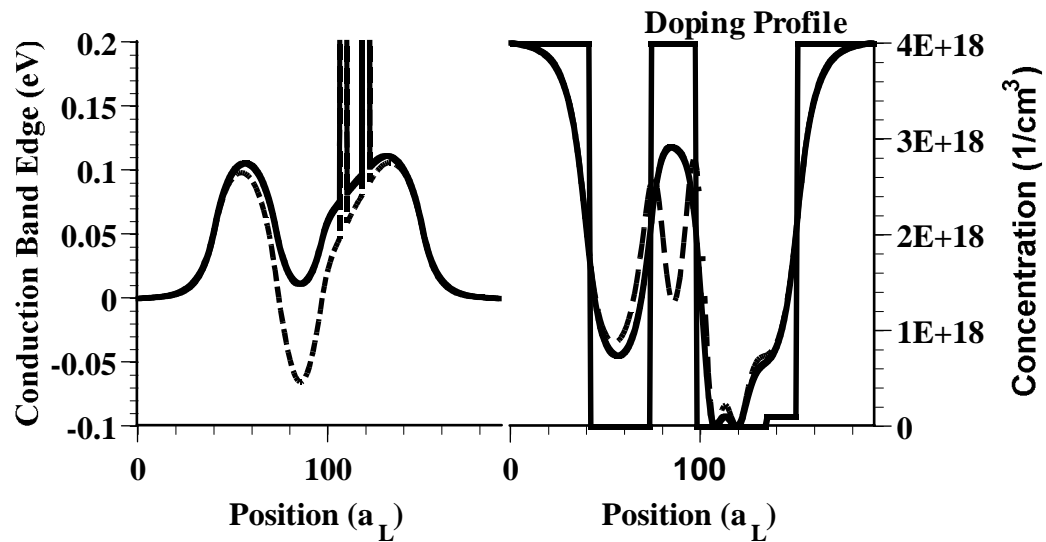
Figure Chapter 6 .2: The Schrödinger Poisson conduction band edges are shown on the left with one potential solution about 0.53 eV below the other. This solution is below the contacts, resulting in quasi-bound states. The concentration in this region is 6.9×10^{17} cm^{-3} lower. The difference in concentration in this region is 1.3×10^{13} cm^{-3}. For this zero bias case both solutions are globally space charge neutral so that the difference in concentration is made up elsewhere in the device.

Chapter 6 .3 QSD modeling and device physics

Much insight into the behavior of quantum well devices can be obtained using a self-consistent Schrödinger - Poisson model. In addition to being the simplest level at which the essential physical processes can be included, the model is also efficient and was the key to discovery of the memory switching phenomena described. In this work both Schrödinger - Poisson models using the effective mass and tight binding approximation may be used. Γ-X mixing in the very thin AlAs layers impacts the potential profiles and the magnitudes of the calculated currents of these devices. Including Γ-X phase space mixing may improve quantitative agreement between simulations and experimental measurements.

It is tempting to optimize our design and understanding of QSDs by doing a broad parametric study of devices with quantum interference effects that may be modulated by varying their charge distribution. To find the optimum device characteristics the parameter space is very large. If the search is limited to a range of total number of layers, thickness of those layers, available pseudomorphic materials, doping concentrations, and carrier type, the sample space, although reduced, is still extremely large. Assuming convergence of an arbitrary model to a solution, an exhaustive search of the potential profile space would be required to demonstrate the lack of a second solution. For this reason parametric studies are limited to specific structures for which assumptions may be reasonably made about some switching characteristics.

Starting from the device structure shown in Figure Chapter 6 .1 a parametric study was done, with its goal an increase in the current ratio between the two solutions. In the interest of keeping the parameter space as small as possible the concentrations and layer thickness in the modulation doped region were varied and current ratios were simulated. The results of this study are shown in Figure Chapter 6 .3 and Figure Chapter 6 .4. A N++ layer concentration of 4e18 and width of 100Å separated from the heterostructure quantum well by 50 Å were chosen.
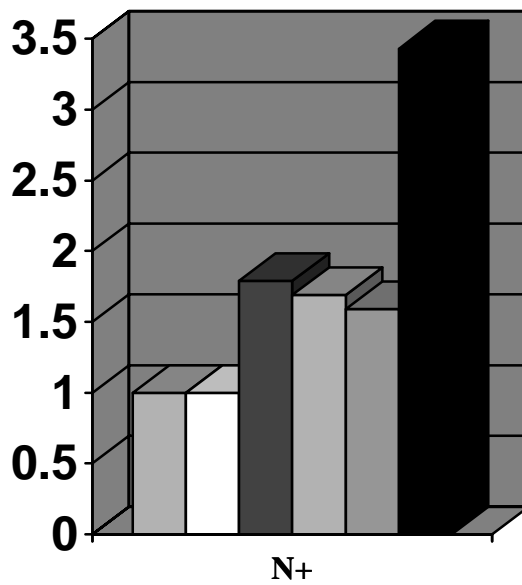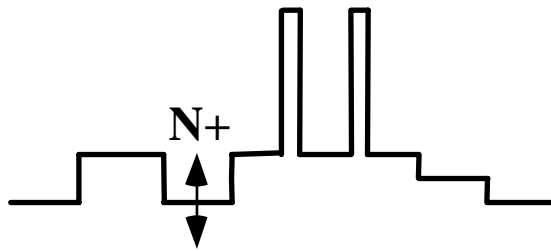
N+

Figure Chapter 6 .3: This parameter study shows the relationship between the N++ layer concentration and the ratio between the currents of the two solutions. The concentrations for the bar chart are from left to right 1e18, 2e18, 4e18, 5e18, 6e18, and 8e18. The 4e18 is the best choice below the solid solubility limit in GaAs. This suggests other materials that support greater concentrations might have larger current ratios.
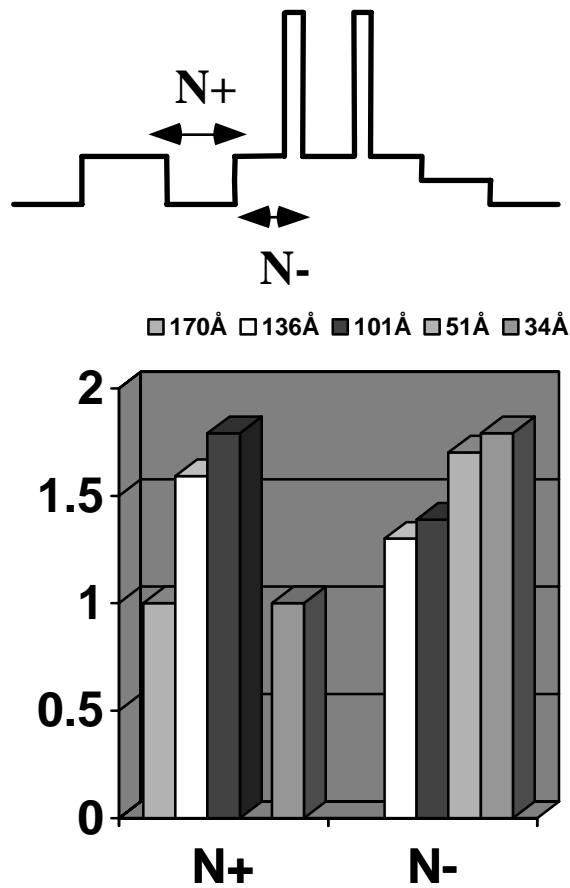
Figure Chapter 6 .4: A parameter study is done to determine the width of the N+ and N- regions. Current ratios are shown in the bar chart for N+ and N- widths of 170Å, 136Å, 101Å, 51Å, and 34Å. Best current ratios are shown for N+ width of 101Å and width of 34Å to 50Å.

The resulting device structure is shown in Figure Chapter 6 .5. A symmetric structure has some advantages in simulation efficiency and higher current ratios between solutions. In addition it may have mixed solutions in one state on one side and a different state on the other. Figure Chapter 6 .6 shows that if the initial potential profile guess is scanned by varying the potential in the

vacinity of the N++ layer, at least three stable solutions result. Each lower potential has a larger number of peaks in the concentration in this layer.

N- 1.0e16 N++ 4.0e18	**N++ contact region** **GaAs**
	N-
	N++ 100 Å
	50 Å N-
17 Å AlAs	N- 50 Å
17 Å AlAs	50 Å N-
	N++ 100 Å
	N-
	N++ contact region **GaAs**

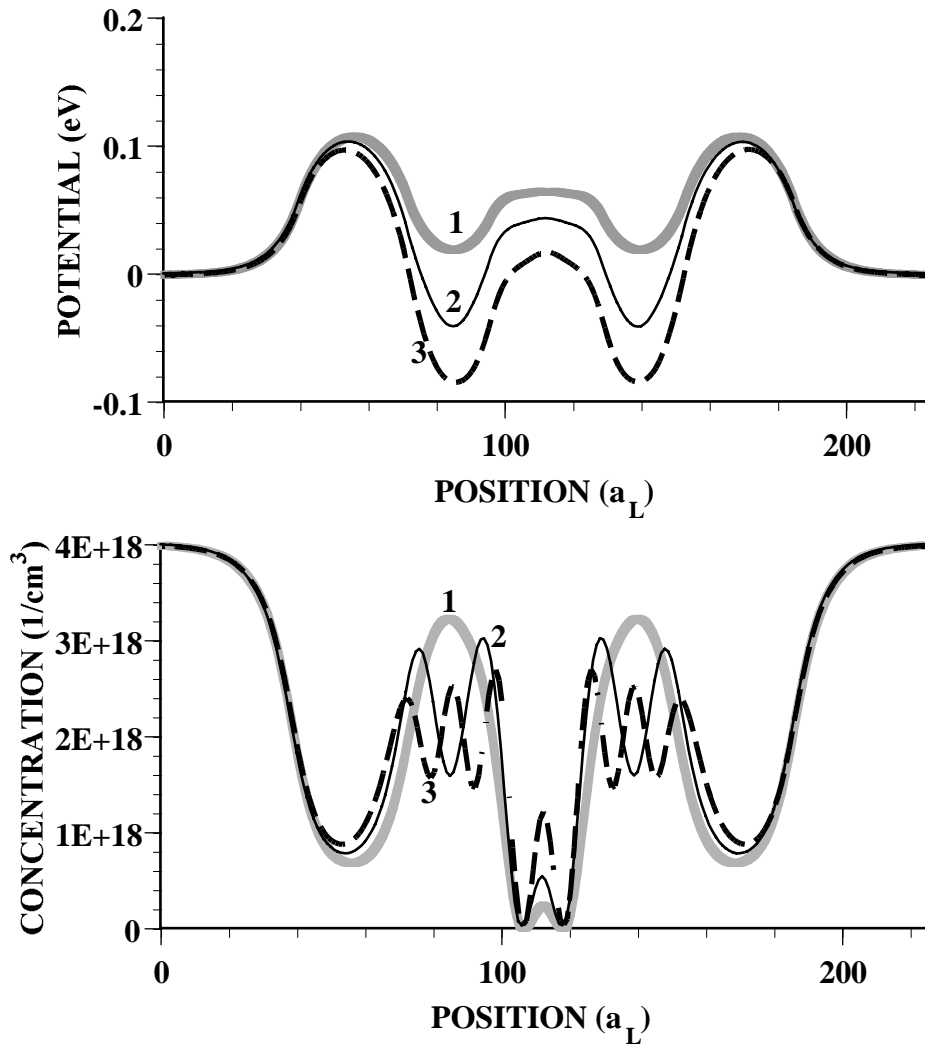Figure Chapter 6 .5: This is a suggested device structure with 100Å N++ region.

107

Figure Chapter 6 .6: The potential profile in the graph on top shows three self-consistent solutions. The solutions with lower potentials in the N++ regions around positions 80 and 140 might be assumed to have lower energy. The lower potential solutions have more oscillatory concentration profiles in these regions. The character of the solutions in the N++ regions suggest a function of DeBrogle wavelengths[62].

Although convergence from one solution to another does not duplicate the dynamics of the physical process, it does provide some understanding of the

development of multiple solutions. Starting with the solution labeled 1 in Figure Chapter 6 .6, and reducing the potential slightly in the vicinity of the N++ layers convergence occurs to the next lower solution. Due to the resonances (shown in Figure Chapter 6 .7 and Figure Chapter 6 .11) between the barriers created by the two N++ regions, the density of states is highly nonlinear. The N- regions near the contacts provide barriers of about 0.1 eV above the contacts. In this case because elastic transport is assumed, electron transport from the contacts through these N- barrier regions is diminished. Carriers between these barriers mainly occur in resonances as shown in Figure Chapter 6 .9. There is a complex interplay between concentration and potential which is unlike that in bulk material governed by a simple density of states function and Fermi Dirac distribution. This causes convergence to even lower potentials eventually including quasi-bound states which occur below the contact conduction band levels. It is the creation of these high concentration states that causes convergence.

The physical process that occurs during switching may be theorized. At high bias the two solutions converge because the resonances and bound states can no longer be supported, resulting in only one solution at high bias and only one at low bias. For an asymmetric device such as the one in Figure Chapter 6 .1, at positive bias charge is concentrated in the N++ layer which characterizes the solution with no quasi-bound states. At negative bias charge is depleted from this layer which characterizes the state containing quasi-bound states. Based on this process, in truly symmetric devices asymmetric states should occur. These asymmetric solutions would be characterized by N++ layers with low

concentrations and potential profiles supporting quasi-bound states on one side of the hetrostructure quantum well and N++ layers with high concentrations and potential profiles not supporting quasi-bound states on the other. Symmetric devices pose a large number of potentially stable states. The challenge is accessing these symmetric and asymmetric solutions.

The character of the solutions in the N++ regions suggest a function of DeBrogle wavelengths[62] which should occur at resonances given by

$$E_r = \frac{h^2}{2 \cdot m^* \lambda^2} \; , \qquad\qquad (\text{ Chapter 6 .1 })$$

where λ is the observed wavelength of the phenomenon. The width of the oscillatory behavior is about 17 nm which corresponds to an energy of about 0.078 ev. Resonances of about 0.08 eV are observed in the zero bias solution shown on the right side of Figure Chapter 6 .7. For the third solution the resonance energy would be around 0.17 ev.

From Figure Chapter 6 .7 and Figure Chapter 6 .11 the density of states at the resonant energies shown peak in the vicinity of the N++ regions. They diminish somewhat in the heterostructure quantum well except for resonances above the N- barriers where the concentration peaks in the heterostructure quantum well and is a node elsewhere.
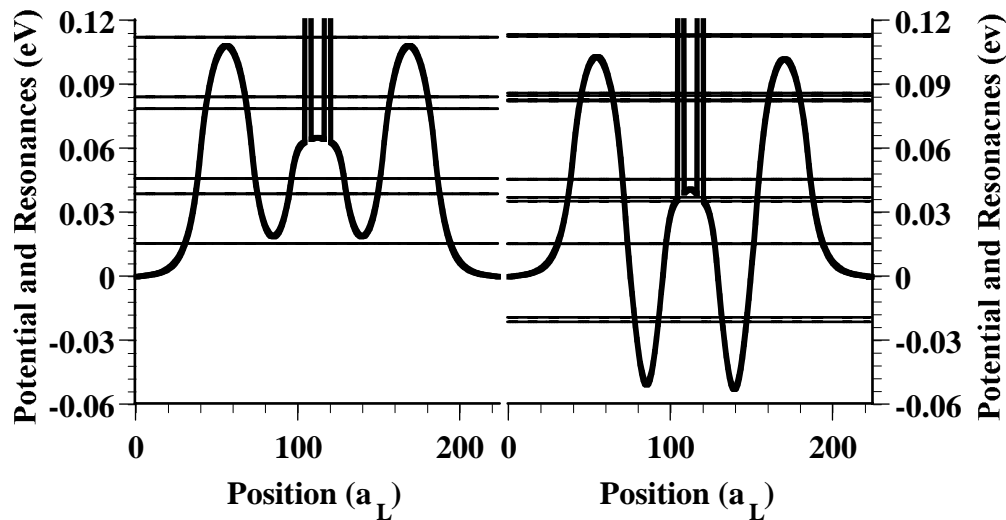
Figure Chapter 6 .7: The plot on the left shows the potential profile for the device structure in Figure Chapter 6 .4. The switched state is shown on the right. The resonant structures are very similar.
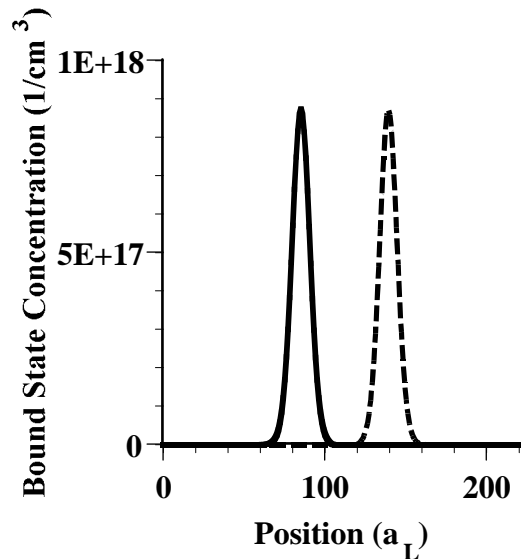

Figure Chapter 6 .8: The second solution shown on the right side of Figure Chapter 6 .7 contains quasi-bound states. The quasi-bound states occur at about -0.02 eV. The concentration in those quasi-bound states is about 8.9×10^{17} cm^{-3} as shown above. The two curves, solid and dashed, are from eigenvectors corresponding to slightly different eigenvalues for the two layers.
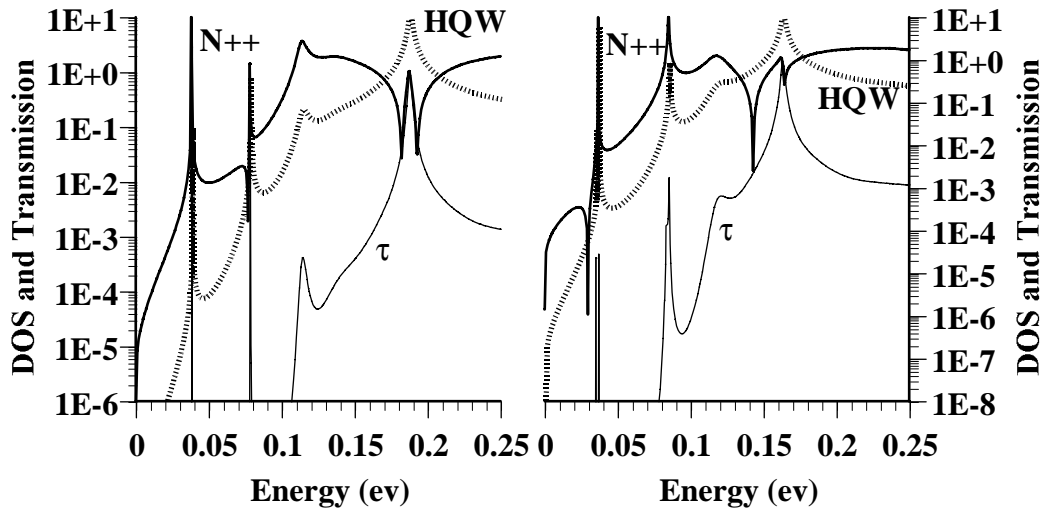
Figure Chapter 6 .9: The graph on the left shows the density of states (DOS) spectrum for the N++ layer and the heterostructure quantum well (HQW). The transmission coefficient (τ) spectra is also shown. The transmission resonance peak is at about 0.18 eV for the solution on the left and 0.16 eV for the solution on the right. These correspond to the left and right solutions above, respectively. At these transmission resonances there is a DOS node elsewhere in the device. The resonance at 0.038 eV in the solution on the left peaks in the N++ regions and is diminished but still a resonance elsewhere. Resonances also occur at about 0.078 eV in the left solution and at about 0.08 eV on the right solution and are diminished in the heterostructure quantum well.

In an attempt to take the effects of Γ-X mixing into account, self-consistent solutions are generated with simple valley to valley coupling [52]. Corresponding self-consistent solutions result. In Figure Chapter 6 .10 concentration profiles corresponding to these two solutions show X valley concentration of about $1X10^{17}$ in the left solution and $2x10^{17}$ cm^{-3} for the right solution. The resulting simulations are very similar to those generated with a Γ only assumption.
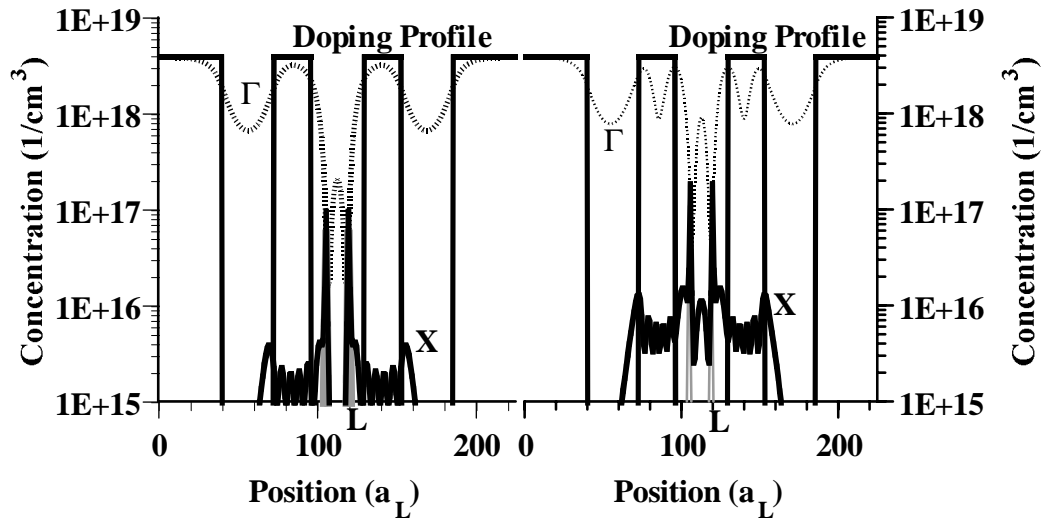
Figure Chapter 6 .10: Γ, X, and L log concentration profiles are shown. Using this coupling parameter the potential profile is very similar to the Γ only case.

Simulations using the tight binding approximation show similar results to those found with the effective mass approximation except that the potential is greater in the heterostructure barrier regions. The concentration in the AlAs barriers are always greater particularly under high bias. Multiple solution characteristics are verified in simulations based on the tight binding approximation.
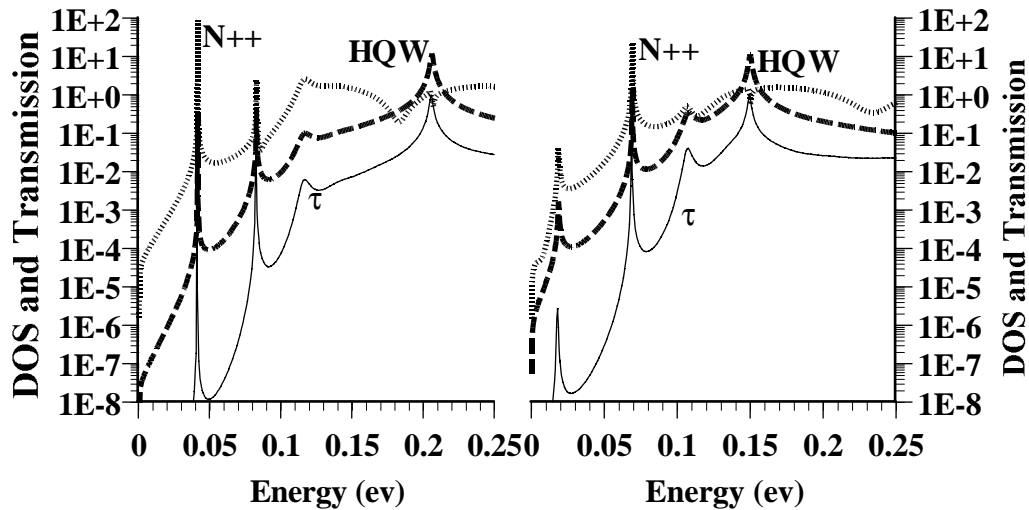
Figure Chapter 6 .11: This is the tight binding DOS and transmission spectra for a tight binding simulation. These curves are very similar to those shown with the effective mass approximation in Figure Chapter 6 .9. Transmission coefficients are generally higher at low energy than with the effective mass approximation. The solution on the left has similar resonances except that the HQW peak is at about 0.2 eV which is about 0.02ev above the corresponding solution in Figure Chapter 6 .9. This is due to the higher potential in that portion of the device for the tight binding solution. The resonances on the right are shifted down about 0.015 eV from those on the right side in Figure Chapter 6 .9.

The tight binding approximation has also been used to examine this phenomenon. The complexity and nonlinearity of the density of states makes convergence to any solution difficult. It may be desirable to search for structures with good convergence characteristics hoping that these would be particularly robust solutions.   The existence of concentration in the barriers causes the solutions to have higher potential in the hetrostructure quantum well region.

Chapter 6 .4 Three terminal multi-state Quantum Storage Device

Current densities during laboratory switching of these devices are on the order of 60 Kamps/cm^2. For a ten by ten micron device switching occurs at 60

114

milliamps and 1.2 volts. The switching power is then 0.072 watts decreasing to 0.014 watts after the state switch. The minimum switching time, determined by the difference in concentration in the N++ layer and the switching current, is about 3.5 ps. Although it leads to a very short switching time the current and power dissipated by the device at switching voltages makes it impractical for high density applications. An alternate method of switching the device from one state to the next at low current would significantly increase its applicability. For this reason there has been some emphasis on developing a three terminal device with improved switching characteristics.

Since the main differences between the solutions occur in the N++ layer; the device might be switched from one state to another by influencing the concentration and potential in the N++ layers directly as shown in Figure Chapter 6 .14, rather than by applying a switching bias. The third terminal, located at the N++ layer, is used only to provide the transients required for switching. Since the top terminal may be used to sense the state and the side terminal to change the state, this is a QSD with separate read and write terminals. It was hoped that this three terminal device would have superior switching performance, enhancing the application of this device for memory and logic functions. The write terminal would normally be left floating and would be used only when a change in the device state is desired. A critical issue for a three-terminal QSD is whether the structural modifications required for fabrication are compatible with the device physics governing operation.

A three terminal implementation of the QSD might be applied to high density memory. A possible circuit implementation consisting of a three terminal QSD vertically integrated with a standard p-n junction diode, is shown in Figure Chapter 6 .12. The diode provides the isolation between the different memory cells but can be included as part of the QSD growth or contact metalization process, not requiring an additional device per memory cell.
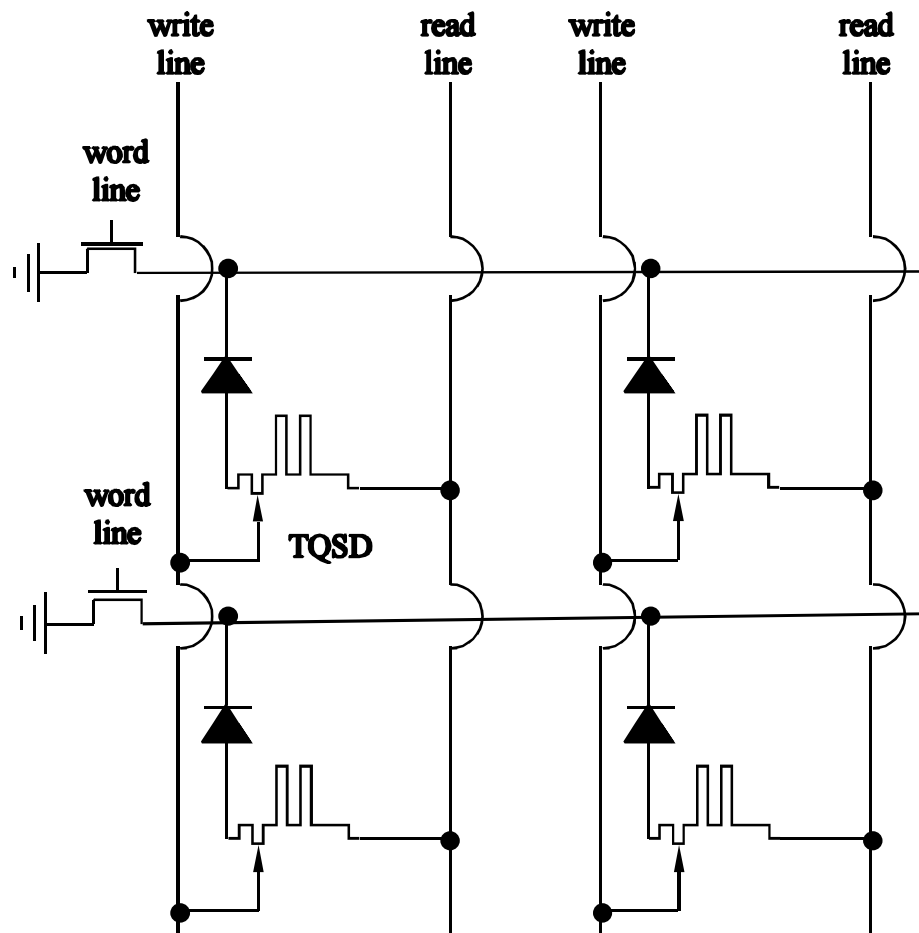
Figure Chapter 6 .12: This is a memory circuit implemented with a three terminal QSD (TQSD). [63]

A three terminal device would be functionally similar to an asynchronous D type flip-flop. If we use a resistive model for the device and require that the input and output be self-compatible (i.e., the output should be sufficient to drive the "write" terminal on the next device) then the required ratio of the resistances produced by the two states of the QSD can be determined. Figure Chapter 6 .13 shows the voltage difference (from the supply or "rail" voltages) produced by the two states as a function of the ratio of their resistances. This indicates we must

achieve a ratio greater than five, but preferably at least ten, to have well separated on and off voltages at the "read" terminal. There does not seem to be significant advantage to ratios greater than about 40. Optimization of our QSD design to achieve such high on-off resistance ratios is a main focus of the proposed parameter study.

Normalized Voltage Offset From Rails $(\Delta V/V_{RAIL})$
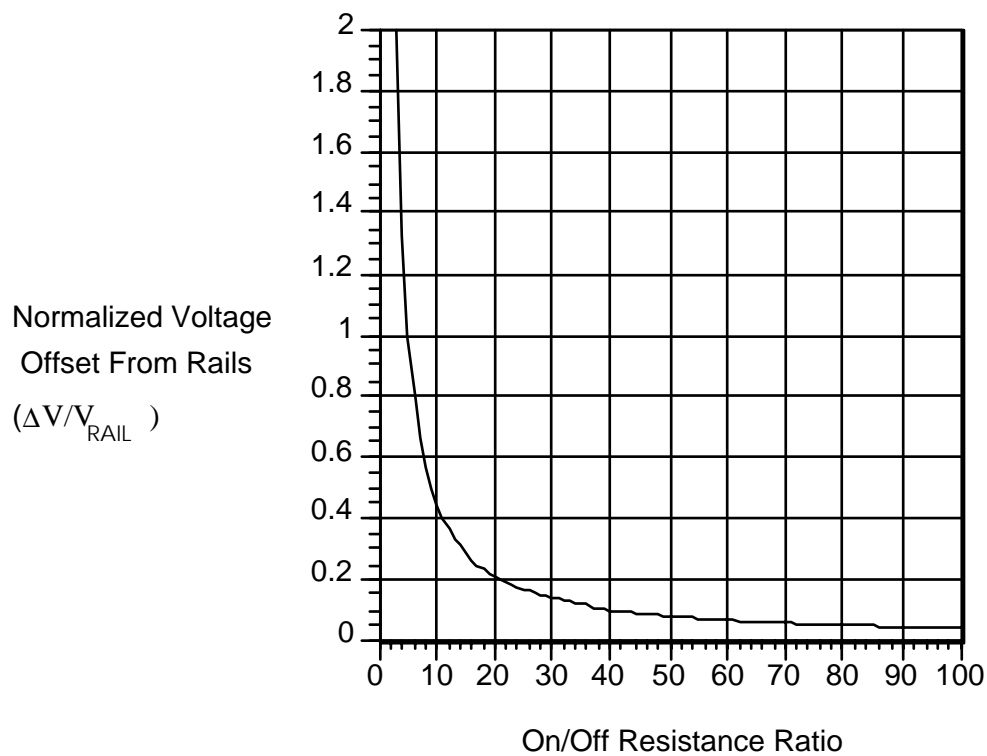
On/Off Resistance Ratio

Figure Chapter 6 .13: This plot shows the advantage of on/off resistance ratio in the performance of a resistance based memory cell.

Ideally the 2/D Schrödinger-Poisson routine described in Chapter 3 could help determine current paths during read and switch operations. This would allow optimization of the design of such a three terminal device.

The fabrication of such a device requires that it be possible to selectively etch down to the N+ layer and deposit the desired metal. Development of the fabrication process requires the addition of an AlAs barrier above the N+ layer. This new device structure shown in Figure Chapter 6 .14 was first suggested by Gullapalli. Using such a structure requires that memory switching be observed in triple barrier resonant tunneling diodes (TBRTDs). The TBRTD device structure shown in Figure Chapter 6 .15 is a simplified version of the three terminal structure.
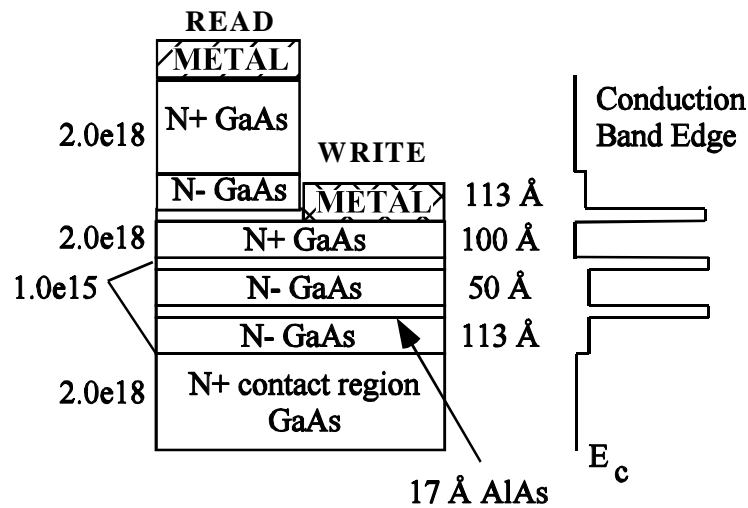

Figure Chapter 6 .14: This is a three terminal triple barrier device structure.

Simulations suggest that multi-state behavior occurs in triple barrier devices as long there is a large space charge region in near proximity to the heterobarrier. Quantum tunneling models developed by our group will be used to optimize device design and determine the behavior of three-terminal versions of the QSD.
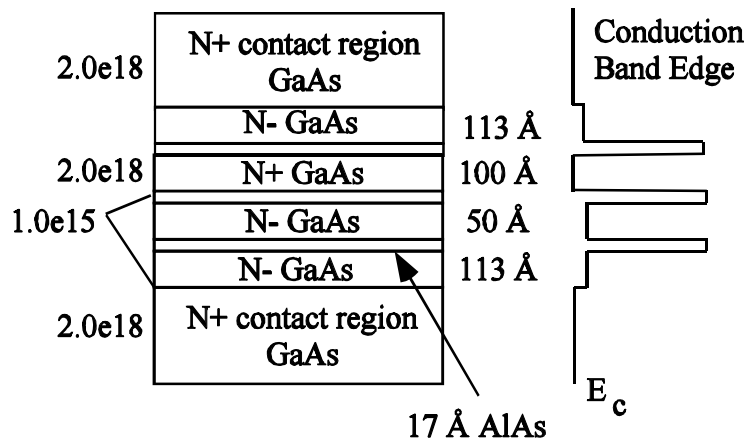
Figure Chapter 6 .15: This is a triple barrier device structure. It is similar to the read terminal structure in the figure above.

A parameter study shown in Figure Chapter 6 .16 has been done to determine widths of the AlAs barriers and of the N+ doped heterostructure quantum well. These results suggest thin barriers 17 Å and a 50 Å N+ doped quantum well. Because of the desire to place a metal contact on top of this layer the N+ thickness is doubled to 100 Å which should only give a slightly lower switching current ratio.
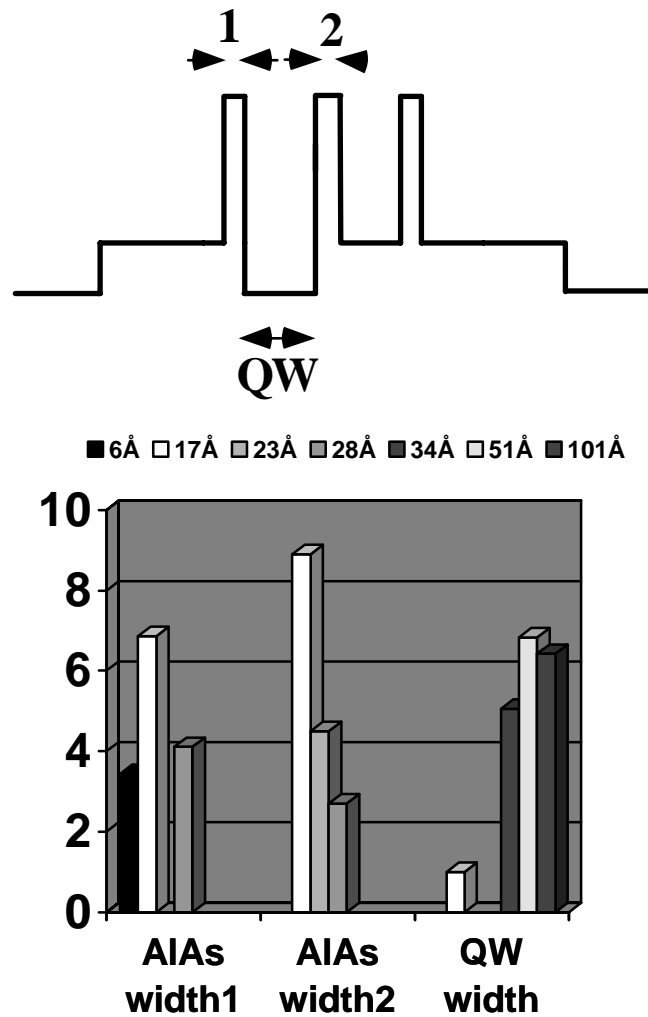
Figure Chapter 6 .16:   These are current ratios between solutions for a range of device structure parameters.   This suggests AlAs barriers of 17Å and QW width of 50Å or 100 Å.

Schrödinger Poisson self-consistent simulations are done of this device using effective mass and tight binding approximations.   Zero bias potential and concentration profiles are shown in Figure Chapter 6 .17.   These profiles show two separate solutions.   More solutions may exist.   As before the concentration is

lower in the state containing quasi-bound states. Multiple solutions are also observed using the tight binding approximation.
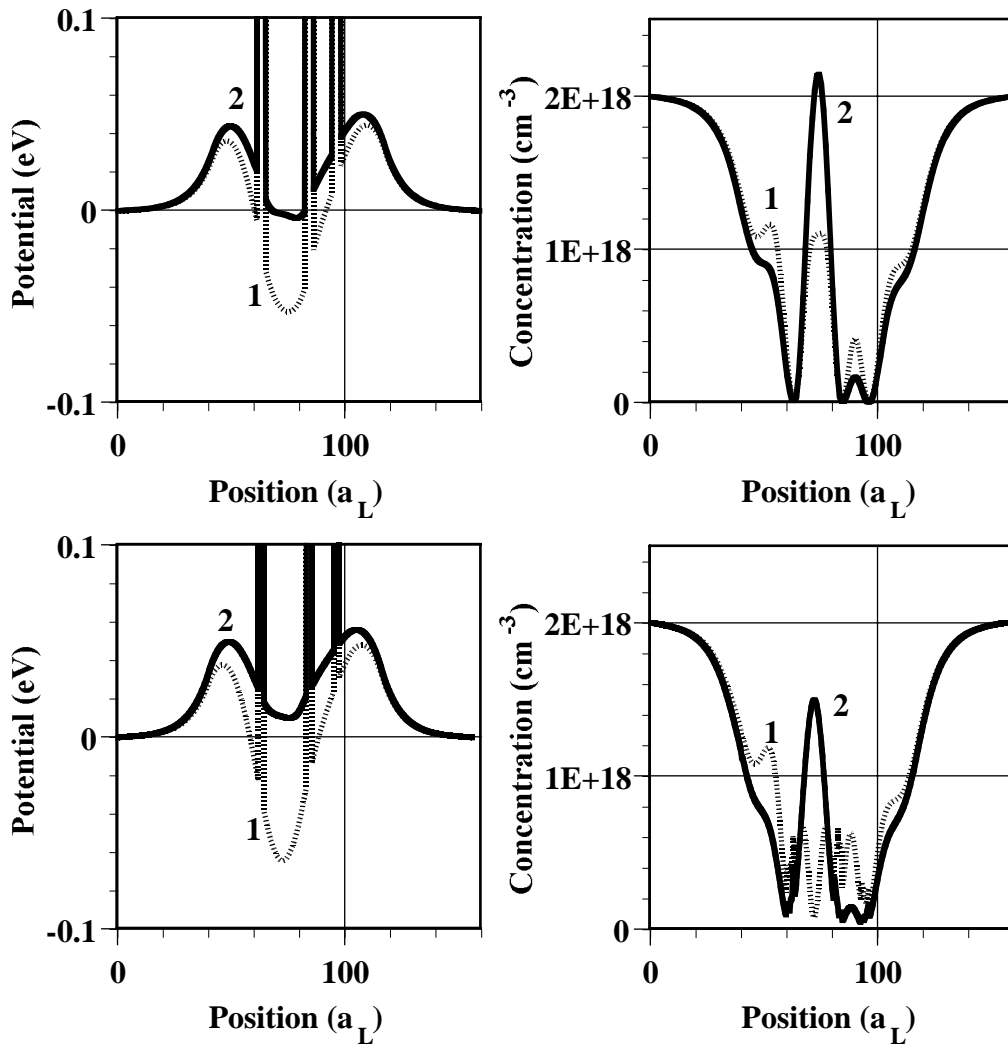
Figure Chapter 6 .17: On the left are potential profiles from self-consistent Schrödinger Poisson solutions and on the right are concentration profiles. Curve 1 is a solution with quasi-bound state solutions and curve 2 is a solution without quasi-bound state solutions. The top two graphs are based on the effective mass approximation and the bottom two are based on the tight binding approximation.

The current density versus bias voltage for these two solutions is shown in Figure Chapter 6 .19. At low bias the two solutions are different but the currents merge at high voltage. The two curves track each other after a given bias and it

may be assumed that two potential profile solutions do not exist above that given bias. In Figure Chapter 6 .18 there appears to be only one solution above about 0.14 and below about -0.15 volts bias. Correspondence between the simulated and measured current density versus bias profiles is poor. Peaks are observed in the simulated solution at about -0.4, -0.36, -0.05, 0.05, 0.1 and 0.45 bias volts. There are inflections in the measured data at about -0.8, -0.2, and 0.2 and a discontinuity at about 0.6 volts. Assuming a voltage drop of 0.15 volts in the laboratory, current peaks for positive bias correspond well. For negative there is not good correspondence between the peaks and the observed inflections. Assuming a 0.15 volt drop in the laboratory the inflections should be observed at -0.2 and -0.55 volts.

Current density simulations based on the tight binding approximation show multiple solutions only at zero and small positive bias (+0.01 volts). At other bias values only solution #1 from Figure Chapter 6 .17 is supported.

Currents at these peaks are much higher in the simulation than in laboratory measurements. For the low bias peaks the ratio between simulated and measured currents is about four. For the high bias peaks the ratio is more than ten.
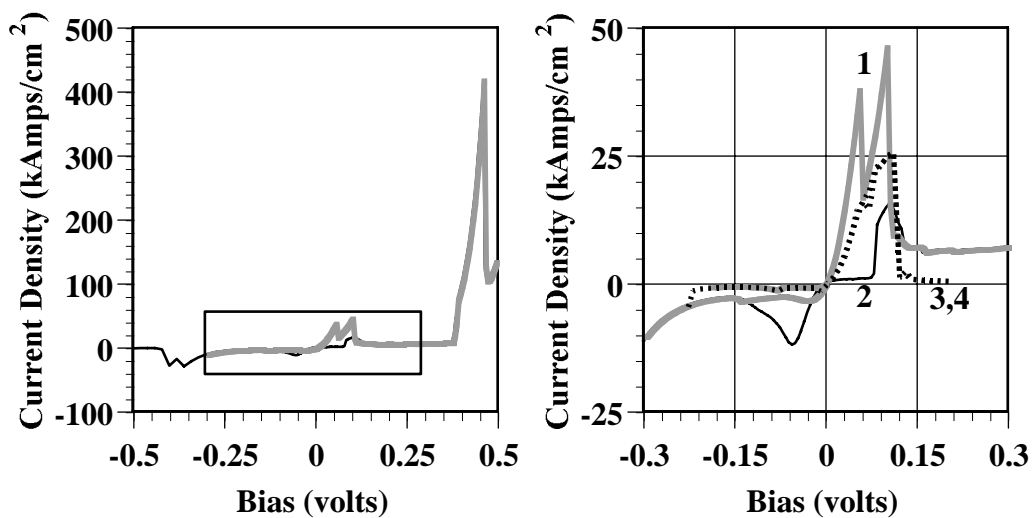
Figure Chapter 6 .18: The current density versus bias voltage plot shows two solutions. The inset region on the box in the curve on the left is shown in the curve on the right. Curve 1 is the quasi-bound state solution, curve 2 is the solution not supporting quasi-bound states. Curves 3 and 4 are tight binding solutions.

Figure Chapter 6 .19: Current density versus bias curves measured in the laboratory show two solutions. Both solutions show inflections suggesting

resonance peaks and valleys. A discontinuity is also shown at about 0.6 volts bias.

Three terminal devices have been fabricated in the laboratory, built on the framework of the TBRTDs described above. Since there is an 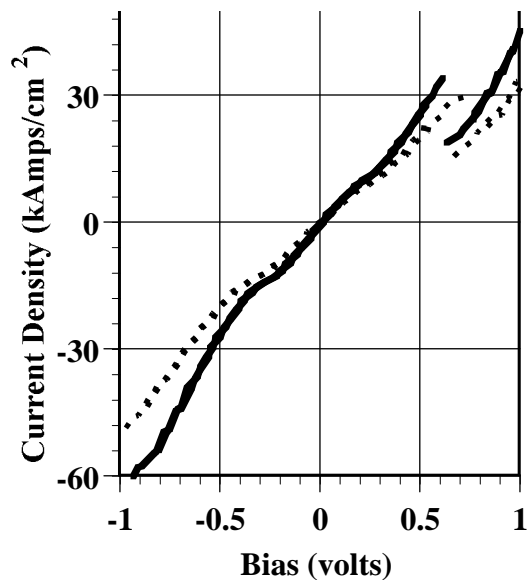unavoidable air interface between the TBRTD structure on the left in Figure Chapter 6 .14 and the write terminal on the right, the N+ layer should tend to be depleted. This is a major failure mechanism for these devices. For this reason a Schottky contact is chosen for the write terminal. It was hoped that by forward or reverse biasing the Schottky contact the N+ layer concentration could be maneuvered near one of the solutions causing the device to settle to that solution when the write pulse is removed. Obviously this is a complex operation.

Fabricated devices were tested for proper electrical relationship between the read write and backside contacts. Only those devices that passed this test were used. None of these devices demonstrated any switching behavior with any bias on the write terminal or with it floating. This problem may potentially be understood by 2D simulation.

Chapter 6 .5 2D Simulations of QSD's

There are two problems that may be solved using the 2D Schrödinger-Poisson routine described in Chapter 3. First, it was hoped that this routine would allow modeling of lateral states and charge movement in two and three terminal devices, which aid in their development and understanding. Simulations of complex 2D structures converge slowly and poorly. Convergence for complex problems has proven to be unlikely. There are a couple of reasons for this. One, the size of real problems overwhelms available resources. Two, the density of

states spectrum is a highly nonlinear function of energy and bias. This is consistent with results obtained by other researchers.

Second, the 2D routine should allow examination of multiple solutions for very thin RTDs. This is important because the understanding of two solutions may be dependent on the physical dimensionallity of the problem. Also, the perspective of using these devices for high density memory requires small devices operate correctly. Very thin 2D DBRTD simulations have failed to converge to a convincing degree. This suggests that for very narrow devices multiple solutions may be limited.

Chapter 6 .6 Summary

Multiple solutions have been shown for several devices in the laboratory and in simulations using the effective mass and tight binding approximations. Although no general conclusion may be drawn from the poor convergence characteristics observed for some devices using tight binding simulations, the lack of multiple solutions observed at high bias suggests that one solution is less stable under these more restrictive assumptions. Generally the effective mass and tight binding approximation simulations differ in the carrier concentration in barrier layers. This results in a different potential solution in this region of the device particularly at high bias. Transmission spectra are higher in the tight binding approximation and show other effects due to valley mixing.

Using this type of simulation other materials and combinations of materials may be used. This will significantly effect design of future devices. To enhance usability improvements should be made in convergence characteristics.

This may lead to simulation based parameter studies capable of optimizing a range of devices.

Bibliography

[1]M. Cahay, M. McLennan, S. Datta *et al*., "Importance of space-charge effects in resonant tunneling devices," Applied Physics Letters **50**, 612 (1987).

[2]W. Pötz, "Self-consistent model of transport in quantum well tunneling structures," Journal of Applied Physics **66** (6), 2458-2466 (1989).

[3]M. J. Paulus, E. T. Koenig, B. Jogai *et al*., "Effects of a low-doped spacer layer in the emitter of a resonant tunneling diode," Superlattices and Microstructures **7** (2), 135-137 (1990).

[4]Vijay P. Kesan, Dean P. Neikirk, Peter A. Blakey *et al*., "The influence of transit time effects on the optimum design and maximum oscillation frequency of quantum well oscillators," IEEE Transactions on Electron Devices **35** (4), 405-413 (1988).

[5]Craig S. Lent and P. Douglas Tougaw, "Lines of interacting quantum-dot cells: A binary wire," Journal of Applied Physics **74(10)** (November 15), 6227-6233 (1993).

[6]Craig S. Lent and P. Douglas Tougaw, "Bistable saturation due to single electron charging in rings of tunnel junctions," Journal of Applied Physics **75(8)** (April 15), 4077-4080 (1994).

[7]K. Nomoto, R. Ugajin, T. Suzuki *et al*., "Single electron photon logic devices using coupled quantum dots: Computation with the Fock ground state," Journal of Applied Physics **79** (1), 291-300 (1996).

[8]P. Douglas Tougaw, Craig S. Lent, and Wolfgang Porod, "Bistable saturation in coupled quantum-dot cells," Journal of Applied Physics **74(5)** (September 1), 3558-3566 (1993).

[9]P. Douglas Tougaw and Craig S. Lent, "Logical devices implemented using quantum cellular automata," Journal of Applied Physics **75(3)** (February), 1818-1825 (1994).

[10]P. Douglas Tougaw and Craig S. Lent, "Logical devices implemented using quantum cellular automata," Journal of Applied Physics **75(3)** (February), 1818-1825 (1994).

[11]P. Douglas Tougaw and Craig S. Lent, "Effect of Stray Charge on Quantum Cellular Automata," Japaneese Journal of Applied Physics **34(1)8b** (August), 4373-4375 (1995).

[12]Ben G. Streetman, *Solid State Electron Devices*, 3 ed. (Prentice Hall, Englewood Cliffs, New Jersey, 1990).

[13]Alwin J. Tsao, "Molecular beam epitaxial growth and fabrication of microwave and photonic devices for hybrid integration on alternative substrates," Dissertation, University of Texas at Austin, 1993.

[14]Chad H. Mikkelson, Alan C. Seabaugh, Edward A. Beam III *et al*., "Coupled-Quantum-Well Field-Effect Resonant Tunneling Transistor for Multi-Valued Logic/Memory Applications," IEEE Transactions on Electron Devices **41** (2), 132-137 (1994).

[15]P. v. d. Wagt and A. Seabaugh, , 1997.

[16]K. Sakai, H. Kawada, O. Takamatsu *et al*., "Electrical Memory Switching in Langmuir-Blodgett Films," Thin Solid Films **179** (1989), 137-142 (1989).

[17]S. M. Gage, J. Hajto, S. Reynolds *et al*., "Anomalous high zero bias resistance in metal amorphous silicon metal structures," Journal of Non-Crystalline Solids **115**, 171-173 (1989).

[18]J.J. Welser, Sandip Tiwari, S. Tiwari *et al*., "Room temperature operation of a quantum-dot flash memory," IEEE Electron Device Letters **18** (6), 278-280 (1997).

[19]K. K. Gullapalli, A. J. Tsao, and D. P. Neikirk, "Multiple self-consistent solutions at zero bias and multiple conduction curves in quantum tunneling diodes containing N^- - N^+ - N^- spacer layers," Applied Physics Letters **62** (7 June), 2971-2973 (1993).

[20]K. K. Gullapalli, A. J. Tsao, and D. P. Neikirk, "Experimental observation of multiple current - voltage curves and zero-bias memory in quantum well diodes with N^- - N^+ - N^- spacer layers," Applied Physics Letters **62** (31 May), 2856-2858 (1993).

[21]K. K. Gullapalli, D. R. Miller, and D. P. Neikirk, "Wigner-Poisson simulation of memory switching heterostructure tunneling diodes," presented at the IEEE International Electron Devices Meeting, Washington, DC, 1993 (unpublished).

[22]K. K. Gullapalli, D. R. Miller, and D. P. Neikirk, "Simulation of quantum transport in memory-switching double-barrier quantum-well diodes," Physical Review B (Condensed Matter) **49** (15 January), 2622-2628 (1994).

[23]O. L. Hartin, D. P. Neikirk, A. Anselm *et al*., "Design and Fabrication of a Three Terminal Quantum Storage Device," presented at the Proceedings IEEE/Cornell Conference on Advanced Concepts in High Speed Semiconductor Devices and Circuits, Ithaca, New York, 1995 (unpublished).

[24] Rolf Landauer, "Need for Critical Assessment," IEEE Transactions on Electron Devices **43** (10), 1637-1639 (1996).

[25] Gerald J. Iafrate and Michael A. Stroscio, "Application of Quantum-Based Devices: Trends and Challenges," IEEE Transactions on Electron Devices **43** (10), 1621-1625 (1996).

[26] J.B. Pendry, A. Pretre, and P.J. Rous, "Causal-surface Green's function method," Surface Science **244** (October 11), 160-176 (1991).

[27] Gerhard Klimeck, Roger Lake, R. Chris Bowen *et al*., "Quantum Device Simulation with a Generalized Tunneling Formula," Applied Physics Letters **67(17)** (October 23), 2539-2541 (1995).

[28] Supriyo Datta, *Quantum Phenomena* (Addison Wesley Publishing Co., Reading, Ma., 1989).

[29] R. Chris Bowen, William R. Frensley, Gerhard Klimeck *et al*., "Transmission resonances and zeros in multiband models," Physical Review B **52,4** (July 15), 2754-2765 (1995).

[30] T. Ando and H. Akera, "Connection of envelope functions at semiconductor heterointerfaces. I. Mixings of gamma and x valleys in GaAs/AlxGa1-xAs," Physical Review B **40** (17), 11619-11632 (1989).

[31] William H. Press, William T. Vetterling, Saul A. Teukolsky *et al*., *Numerical Recipes in C*, 2nd ed. (Cambridge University Press, Cambridge, Mass., 1992).

[32] David S. Watkins, "Some perspectives on the eigenvalue problem," Society for industrial and Applied Mathematics **35** (3), 430-471 (1993).

[33] David Kincaid and Ward Cheney, *Numerical Analysis* (Brooks/Cole Publishing Co., Pacific Grove, California, 1991).

[34] G.H. Golub and C.F. Van Loan, *Matrix Computations* (John Hopkins University Press, Baltimore, 1989).

[35] Claude Cohen-Tannoudji, Bernard Diu, and Frank Laloe, *Quantum Mechanics*, 2nd ed. (John Wiley and Sons, New York, 1977).

[36] C. Reinsch and J.H. Wilkinson, *Handbook for Automatic Computation* (1971).

[37] D. Z.-Y. Ting, E. T. Yu, and T. C. McGill, "Multiband treatment of quantum transport in interband tunnel devices," Physical Review B (Condensed Matter) **45** (7), 3583-3592 (1992).

[38] H.A. Van Der Vorst, "BI-CGSTAB: A Fast and Smoothly Converging Variant of BI-CG for the Solution of Nonsymmetric Linear Systems," SIAM Journal of Scientific Statistical Computing **13** (2), 631-644 (1992).

[39]D. R. Kincaid and D. M. Youg, "A brief review of the ITPACK project," Journal of computational and applied mathematics **24** (1/2), 121 (1988).

[40]Kenneth S. Kundert and Alberto Sangiovanni-Vincentelli, Documentation Report No. Version 1.3a, 1988.

[41]Kiran K. Gullapalli, "Heterostructure Device Simulation using the Wigner Function," Dissertation, University of Texas, 1994.

[42]Grehard Klimeck, Roger Lake, R. Chris Bowen *et al.*, "Nemo: A General Purpose Quantum Device Simulator," presented at the Texas Instruments Research Colloquium, Dallas, TX, 1996 (unpublished).

[43]Yuming Hu and Shawn Stapleton, "Self-consistent model of a double barrier resonant tunneling diode: Dependence of intrinsic bistability on structural parameters," Journal of Applied Physics **73** (10), 5254-5263 (1993).

[44]N. W. Ashcroft and N. D. Mermin, *Solid State Physics* (Saunders College, Philadelphia, 1976).

[45]P. Vogl, "A Semi-Empirical Tight-Binding Theory of the Electronic Structure of Semiconductors," Journal of the Physical Chemistry of Solids **44** (5), 365-378 (1983).

[46]Timothy B. Boykin, Jan P. A. van der Wagt, and James S. Harris, "Tight-binding model for GaAs/AlAs resonant tunneling diodes," Physical Review B **43** (6), 4777-4784 (1991).

[47]O. Madelung, "Semiconductors group IV elements and III-V compounds," in *Data in Science and Technology*, edited by R. Poerschke (Springer-Verlag, New York, 1991), Vol. I.

[48]Sadao Adachi, "Properties of Aluminum Gallium Arsenide," in *EMIS Data Reviews Series* (INSPEC, the Institution of Electrical Engineers, London, 1993), Vol. 7, pp. 299.

[49]T. Saito, Y. Hashimoto, and T. Ikoma, "Band discontinuity in GaAs/Alas superlattices with InAs strained insertion-layers," Superlattices and Microstuctures **15** (4), 405-407 (1994).

[50]A. Mujica and A. Munoz, "Self Consistent Tight-Binding Calculations of Band offsets in GaAs/AlxGa1-xAs-(110) and GaSb/AlxGa1-xSb-(110) Heterojunctions - Theoretical Evidence for a New Common-Anion Rule," Solid State Communications **81** (11), 961-963 (1992).

[51]G. Platero, J. Sanchez-Dehesa, C. Tejedor *et al.*, "Electronic structure of (100) semiconductor heterojunctions," Surface Science **186**, 553-557 (1986).

[52]J.P. Sun, R.K. Mains, K. Yang *et al*., "A self-consistent model of Γ-X mixing in GaAs/AlAs/GaAs quantum well structures using the quantum transmitting boundary method," Journal of Applied Physics **74** (8), 5053-5060 (1993).

[53]Timothy B. Boykin and Jr. James S Harris, "X-Valley tunneling in single AlAs barriers," Journal of Applied Physics **72** (3), 988-992 (1992).

[54]Yia-Chung Chang and J. N. Schulman, "Complex band structures of crystalline solids: and eigenvalue method," Physical Review B **25** (6), 3975-3986 (1982).

[55]J. N. Schulman and Yia-Chung Chang, "Reduced Hamiltonian method for solving the tight binding model of interfaces," Physical Review B **27** (4), 2346-2354 (1983).

[56]R. Beresford, L. F. Luo, and W. I. Wang, "Resonant tunneling through X-valley states in GaAs/AlAs/GaAs barrier heterostructures," Applied Physics Letters **55** (15), 1555-1557 (1989).

[57]D. Landheer, H. C. Liu, M. Buchanan *et al*., "Tunneling through AlAs barriers: Γ-X transfer current," Applied Physics Letters **54** (18) (1989).

[58]Nick Moll, Mark R. Hueschen, and Alice Fischer-Colbrie, "Pulse_Doped AlGaAs/InGaAs Pseudomorphic MODFET's," IEEE transactions on Electron Devices **35** (7), 879-886 (1988).

[59]K. K. Gullapalli, A. J. Tsao, and D. P. Neikirk, "Observation of zero-bias multi-state behavior in selectively doped two-terminal quantum tunneling devices," presented at the IEEE International Electron Devices Meeting, San Francisco, CA, 1992 (unpublished).

[60]K. K. Gullapalli and D. P. Neikirk, "Incorporating spatially varying effective-mass in the Wigner-Poisson model for AlAs/GaAs resonant-tunneling diodes," presented at the Third Annual International Workshop on Computational Electronics, Portland, OR, 1994 (unpublished).

[61]K. K. Gullapalli, "Heterostructure Device Simulation using the Wigner Function," Ph. D., The University of Texas at Austin, 1994.

[62]E. F. Schubert and Klaus Ploog, "Electron Subband Structure in Selectively Doped n-AlxGa(1-x)As/GaAs Heterostructures," IEEE Transactions on Electron Devices **32** (9), 1868-1873 (1985).

[63]D. P. Neikirk, NSF Proposal , 1994.